Influence of Al2O3-13TiO2 powder on a C45 steel using atmospheric plasma spray process

G Mahu[1], C Munteanu[1]*, B Istrate[1], M Benchea[1] and S Lupescu [1]

[1] "Gheorghe Asachi" Technical University of Iasi, Faculty of Mechanical Engineering, 43 "D. Mangeron" Street, 700050, Iasi, Romania

E-mail: cornelmun@gmail.com

Abstract. In automotive industry, we encounter conventional treatments for the protection of crankshaft journals, such as induction, nitridization, carburization or chrome plating. This study aims to analyze the sprayed layers using an atmospheric spray plasma coating method on the surface of C45 steel specimens used in crankshaft construction, with the Spraywizard 9MCE installation. The Al2O3-13TiO2 powder was used for the coating. The sprayed layers were analyzed microstructured and morphologically by means of optical and electronic microscopy as well as X-ray diffraction. Indentation and microscratch tests were performed to study the adhesion of sprayed layers on the base material. It has been observed from the analyzed samples that the layers obtained by spraying with Al2O3-13TiO2 are superior in terms of hardness compared to the base material. The layers have a morphological appearance of compact nature and have a good adhesion to the base material. The study reveals that spraying of appropriate powders into the plasma jet can be an alternative to classical thermal treatments on the crankshaft journals.

1. Introduction

Crankshafts are the most stressed parts of the internal combustion engine. To increase durability, wear resistance and contact fatigue resistance, various thermal treatments are applied to the surface of the crankpin journals and main journals, such as nitriding, carburizing, chromating, carbonitriding, etc. [1, 2]. The most commonly used thermal deposition process is the plasma jet deposition [2, 3]. T. Bell and H. Liu conducted a study on plasma deposition on a C45 steel surface, the most common plasma deposition method being nitriding according to the study [4,5]. Through the plasma jet spraying process, resistance to wear, corrosion and high temperature coatings on the surface of a material improves their properties, so the method is very effective [6].

The purpose of this study is to highlight the properties of sprayed layers by the plasma spray technique on the surface of a C45 steel compared to the base material from the microstructure, X-ray diffraction point, microscratch test and Young's modulus . A very important element in the plasma jet spraying process is the deposition parameters. Żórawski W and colleagues conducted a study on sprayed layer of Al2O3TiO2 in plasma jets, so the nanostructural analysis as well as the tests performed revealed that important changes in the properties of the deposited layers can occur, so the layer hardness values can vary from 611 HV to 772 HV for a current variation of 550A to 650A [7,8,9].

2. Experimental

For this study, the alloy used is a C45 steel having the components listed in Table 1:

Table 1. C45 composition

C45	C	Si	Mn	S	P
%	0.45	0.17	0.52	0.031	0.032

For the analysis, 4 samples of 30 mm x 10 mm x 2 mm were cut, and then they were sandblasted. The Metco 130 powder was sprayed with the SPRAYWIZARD 9MCE plasma spray jet device produced by Sulzer & Metco having the chemical formula Al2O3-13TiO2. The deposition performed has the spray parameters shown in Table 2. The samples were prepared metallographically for the study of the microstructure using 200, 500, 800 or 1200 abrasive paper, after which they were cleaned with ethyl alcohol and chemically attacked with 2% nital agent.

The powder used for the spraying has the components in Table 2:

Table 2. Powder composition

Product	Chemical composition (nominal wt. %)	
	TiO2	Al2O3
Metco 130	13	87

Table 3. Spray parameters

Powder	**Metco 130**
Spray distance (mm)	100
Injector	1.8
Curent Intensity (A)	600
Electric arc voltage (U)	75
Rotation speed (rpm)	55
Argon flow (m3 / h)	50
Hydrogen flow (m3 / h)	14

In order to analize the microstructure and morphology of the specimens, optical and electronic microspots were used. The Leica DMI5000 M microscope was used for electron microscopy, with a Leica HCS optical system and an enhanced power of 1.5X to 250X.

For electronic microscopy, the SEM QUANTA 3D Dual Beam microscope was used, being produced by the Dutch FEI. The QUANTA microscope is equipped with High Vacuum mode using the Large Field Detector (LFG) detector, resulting in enhanced 500X, 1000X, and 5000X images with a working distance of about 15 mm [11]. Testing of adhesion on the surfaces of the deposited layers was performed by microscratch and indentation methods by means of the CETR UMT-2 tribometer equipped with a DFH-20 Dual Friction / Load Sensor, on which a blade with a radius of 0.4 mm. The indenting speed was 10mm / min. The X-ray diffractometer, X 'Pert Pro MRD, performed X-ray diffraction [12]. The device was equipped with an X-ray tube with Cu kα, λ = 1,54 Å using a voltage of 45KV of 40mA, the diffraction angle (2θ) ranging between 25 and 130º.

3. Results and discussions

3.1. Microstructural analysis

In Figure 1 we can see the SEM images of the layer obtained by spraying the Metco 130 Al2O3-13TiO2 powder. In Figure 1b, variations in layer thickness can be observed. Values vary in the range 279-306μm. The spraying had a uniform distribution on the surface of the samples, respecting the powder manufacturer's spraying specifications. There is a porous structure with few microcracks (Figure 1e) and unmelted particles (Figure 1d). Morphology of the powder reveals a compact structure with splats (Figure 2c). The layer is adherent to the material and after the microscratch process the layer has not been destroyed, although it has been sprayed directly on the surface without an intermediate layer. In Figure 2, we can see SEM images of the base material, C45 steel. It is highlighted a ferro-perlitic structure, with equiaxial grains, relatively uniform with small granulation. Small inclusions, isolated, with tendencies of segregation, are observed.

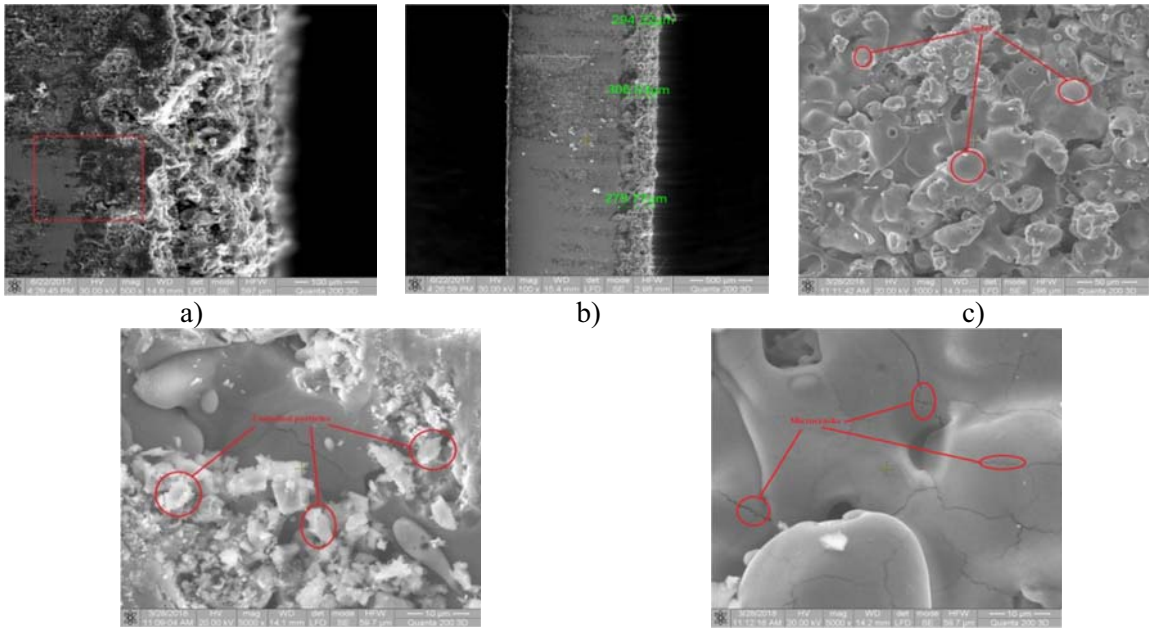

a) b) c)

d) e)

Figure 1 SEM images of the deposited Metco 130-Al2O3-13TiO2: a) layer separation zone, b) layer thickness, c) layer structure (1000X), d, e) layer structure (5000X).

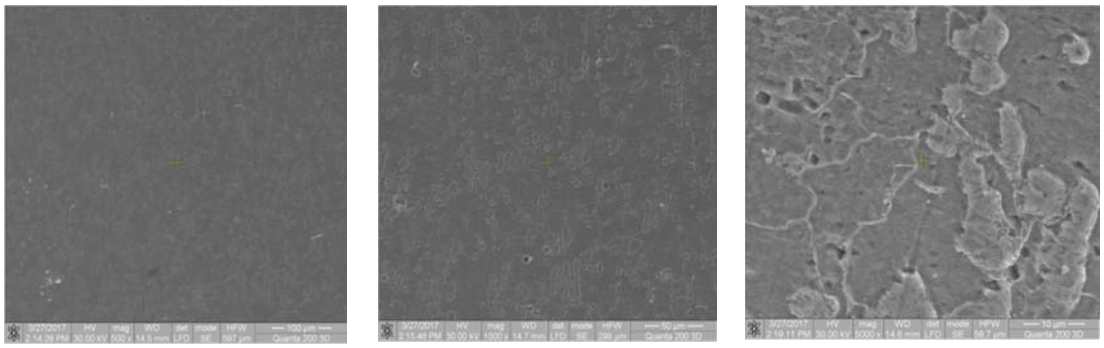

a) b) c)

Figure 2 SEM images of C45 base material; images magnified at: a) 500X, b) 1000X, c) 5000X.

3.2. XRD analysis

The predominant phases identified in Figure 3a for the Metco130 powder of Al2O3 have characteristic peaks at 25.56 ° angles; 35.14 °; 43.34 °; 57.48 ° and 68.18 °. Al2O3 is identified by a crystalline structure of the rhombohedral type.

TiO2 is evidenced by two rutile and anatase forms (rutile and anatase) having characteristic peaks at 25.34 °, 25.69 °, 30.8 °, 48.04 ° and 55.24 ° angles. Rutile and anatase have a tetragonal structure.

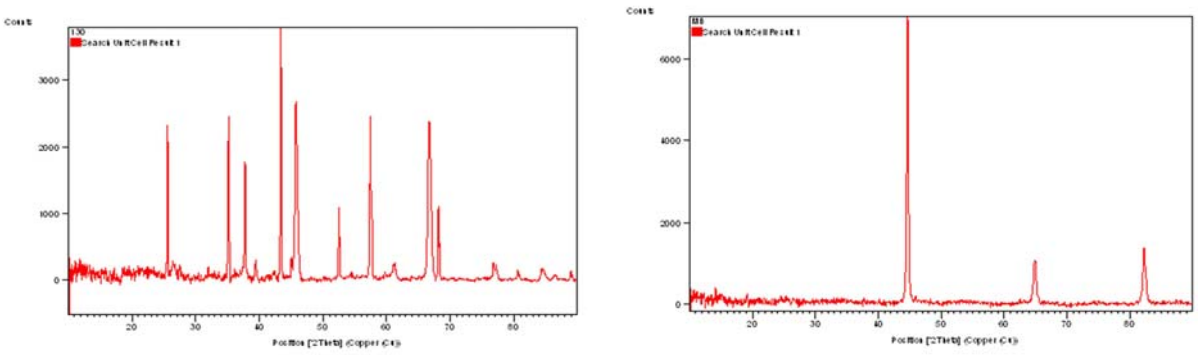

a) b)

Figure 3 X-ray diffractogram, diffraction range: 20 = 20 ... 100 °:
a) Metco130, b) Base material.

In Figure 3b we observe Fe with a cubic crystal structure, having peaks characteristic at angles 44.66°, 65.00 °, 82.31 °.

3.3. Microindentation analysis

Figure 4 shows the variation curves of penetration force in ratio with the depth of indentation after the Microindentation Test for Metco 130 and the base material. The maximum force with which the indent was operated was 9N for all samples.

It can be noticed that the indentation depth for the samples sprayed with Metco 130 have lower values, compared with the indentation of the samples from the base material, even from very low values of the indentation force. The hardness of the sprayed Metco 130 layer is superior to the base material.

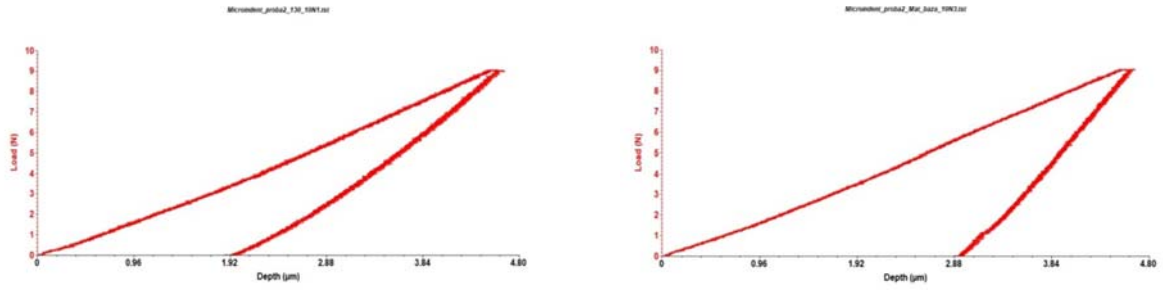

a) b)

Figure 4 Penetration variations in relation to the depth of indentation:
a) Metco 130, b) Base material.

The coefficient of friction measured on samples covered with the Metco 130 powder has higher values than the base material. The friction coefficient variation diagrams can be seen in Figure 5.

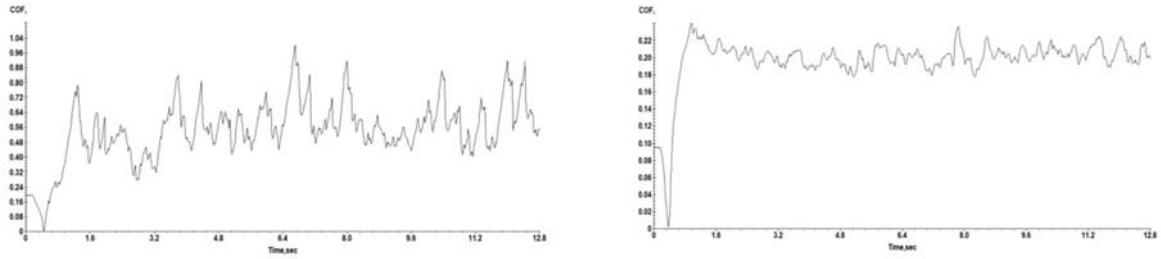

a) b)

Figure 5. Chart of the COF variation: a) Metco 130; b) Base material.

Table 4. Samples parameters

Powder	Hardness (GPa)	COF	Stiffness(N/µm)	Young's Modulus (GPa)
Metco 130	2.3425	0.5971	4.295	61.467
Base Material	2.0387	0.1996	6.136	83.34

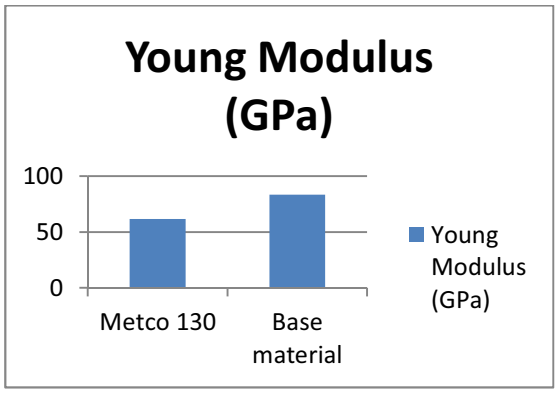

Figure 6. The elastic modulus parameters for Metco 130 and the base material.

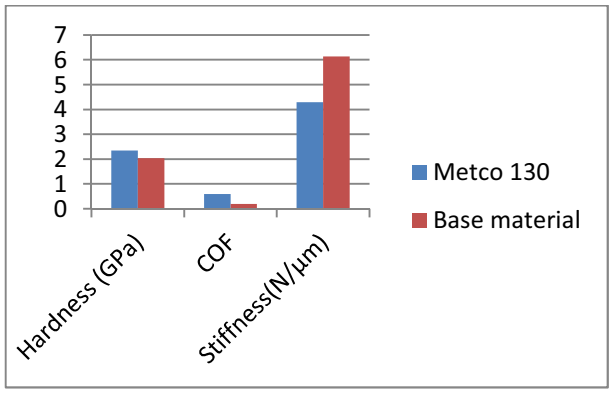

Figure 7. Comparative chart for parameters obtained from the microscratch test for Metco 130 and the base material.

Samples covered with Metco 130 show higher values of the hardness of the deposited layer compared to the base material (Figure 7). For the modulus of elasticity, the samples covered with Metco 130 have maximum values of 61.467 GPa compared to 83.340 GPa obtained with the base material (Figure 6).

4. Conclusions

1) Following the microscopic analysis of the layers deposited with Metco 130 we can say that the plasma deposition method is an efficient method, the deposited layers being hard, having a low porosity, and no major defects, only isolated microcracks, splats and unmelted particles.
2) The layers sprayed with Metco 130 have a complex microstructural feature and do not require the intermediate layer to be deposited on the base material, respecting the manufacturer's specifications, so that the cost of the process does not increase compared to that in which intermediate layers are used in the spraying process.
3) The friction coefficient for Metco 130 is superior to the base material. The values of the elasticity modulus for the Metco 130 pulverized samples are inferior to the base materials, but the hardness of

the deposited layers is superior to the base material, which is very important in the event of lubrication problems or defects in the main bearing or rod bearing.
4) The plasma jet deposition process may be an interesting alternative to classic thermal treatment methods for crankshafts, given the conclusions outlined above, especially for crankshafts built in small series.

References

[1] Hermann H, Sampath S and McCune R 2000 Thermal Spray: Current status and future trends *Volume* **25** pp 17-25
[2] Tudose-Sandu-Ville O F 2016 Study on the deterioration origin of thermomechanical contact fatigue IOP Conference Series: Materials Science and Engineering **147 (1)** 012007
[3] Beardsley M B, Happoldt P G and Kelley K C 1999 Thermal Barrier Coatings for Low Emission, High Efficiency Diesel Engine Applications *SAE International*
[4] Istrate B, Munteanu C, Matei M, Oprisan B, Chicet D and Earar K 2016 Influence of ZrO_2 - Y_2O_3 and ZrO_2-CaO coatings on microstructural and mechanical properties on Mg-1,3Ca-5,5Zr biodegradable alloy *IOP Conference Series: Materials Science and Engineering* vol **133** 012010
[5] Bell T,Sun Y and Suhadi A 2000 *Vacuum* **59** 14-23.
[6] Liu H, Li J C, Sun F and Hu J 2014 *Vacuum* **109** 170-174
[7] Ahangarani Sh, Mahboubi F and Sabour A R 2006 *Vacuum* **80** 1032
[8] Rahim A, Sahaba M, Saadb N H, Kasolangb S and Saedonb J 2012 Impact of Plasma Spray Variables Parameters on Mechanical and Wear Behaviour of Plasma Sprayed Al2O3 3%wt TiO2 Coating in Abrasion and Erosion Application, *Procedia Engineering* **41** 1689 – 1695
[9] Żórawski W, Góral A, Bokuvka O, Berent K 2013 Microstructure and mechanical properties of plasma sprayed nanostructured and conventional Al2O3–13TiO2 coatings, *Proceedings of the International Thermal Spray (ITSC) Conference*. Busan, Republic of Korea
[10] Kim G E 2011 Thermal Sprayed Nanostructured Coatings: Applications and Developments, *Perpetual Technologies, Inc., Ile des Soeurs*, Quebec, Canada 91-92
[11] Manea L R, Scarlet R and Sandu I 2015 Analysis of Electrospun Nanofibers Flaws from Polymeric Solution of Polyetherimide, *Rev. Chim. (Bucharest)* **66(10)** 1622-1627
[12] Manea L R Cramariuc B, Scarlet R, Cramariuc R, Sandu I and Popescu V 2015 Equipment for Obtaining Polimeric Nanofibres by Electrospinning Technology II. The obtaining of polimeric nanofibers *Mat. Plast.(Bucharest)* **52(2)** 180-185